Microstructures and mechanical properties of bulk nanocrystalline silver fabricated by spark plasma sintering

Hu Wang
School of Materials Science and Engineering, Beijing Institute of Technology, Beijing, 100081, People's Republic of China

Xing-Wang Cheng and Zhao-Hui Zhang[a)]
School of Materials Science and Engineering, Beijing Institute of Technology, Beijing, 100081, People's Republic of China; and National Key Laboratory of Science and Technology on Materials under Shock and Impact, Beijing, 100081, People's Republic of China

Zheng-Yang Hu and Sheng-Lin Li
School of Materials Science and Engineering, Beijing Institute of Technology, Beijing, 100081, People's Republic of China

(Received 9 March 2016; accepted 16 May 2016)

Bulk nanocrystalline (NC) silvers were fabricated by spark plasma sintering process. The effects of sintering temperature on physical and mechanical properties of the NC silvers were investigated. The results indicate that no impurities were introduced into the bulk compacts during the preparation procedure. Both the density and the electrical conductivity of the NC Ag increase with an increase in sintering temperature. However, the micro-hardness and ultimate tensile strength (UTS) of the bulk compacts increase initially and then decrease with increasing sintering temperature. The NC Ag sintered at 500 °C exhibits the highest micro-hardness of 85.3 HV along with the best compression yield strength of 379 MPa and the highest UTS of 534 MPa. The deterioration of the mechanical properties of the NC Ag sintered at 550 °C should be attributed to the rapid grain growth.

I. INTRODUCTION

Bulk nanocrystalline (NC) materials are polycrystalline materials consisting of grains in a nanometer range from 1 to 100 nm. They were widely studied in the past few decades due to their unusual mechanical properties and outstanding physical and chemical properties.[1–4] In particular, a conventional metal can get a 7-fold or even decuple increase in tensile strength when the grain size reaches the nanoscale, assumably due to the grain-boundary strengthening mechanism known as the Hall–Petch effect.[2] For example, tensile strengths as high as 1.5 GPa in NC-iron and 0.28 GPa in NC-aluminum have been reported.[5,6] According to the mechanism of fine-grain strengthening, the plasticity of NC materials can also be increased. However, the bulk NC materials usually exhibit undesirable low ductility, especially for the NC metals fabricated by powder metallurgy method. Thus, the fabrication of the NC materials with both high strength and good ductility has become a hot research focus in recent years.[7–11]

Up to now, many techniques have been developed to fabricate bulk NC materials, such as severe plastic deformation,[12–16] crystallization of amorphous solids,[17] powder metallurgy,[18,19] etc.[20–22] In these methods, powder metallurgy is considered to be suitable to fabricate the bulk NC materials due to its simplicity and feasibility. However, this method is hard to generate NC materials with controllable, stable, and homogeneous nanostructures because the metal nanoparticles are easy to get coarse during the conventional powder metallurgy process. Spark plasma sintering (SPS) technology combines with hot-pressing sintering, resistance heating, and plasma activation.[23–25] As a result, SPS technology has many extraordinary advantages such as fast heating speed, short heat preservation time, and low sintering temperature etc.[3,26–28] Thus, grain growth of the bulk compact can be effectively hindered.[27,29] In addition, the relatively high compressive stress applied in the SPS leads to a better contact between powder particles, which can enhance the existing densification mechanisms such as grain boundary diffusion, lattice diffusion, and viscous flow, or activate new mechanisms.[30] These facts make SPS process quite suitable for fabricating NC materials with both high strength and excellent plasticity.[6]

Silver is well known to be antimicrobial, antioxidation, and hot corrosion resistance, thus it is promising to use

Contributing Editor: Jürgen Eckert
[a)]Address all correspondence to this author.
e-mail: zhang@bit.edu.cn
DOI: 10.1557/jmr.2016.212

 © Materials Research Society 2016

https://doi.org/10.1557/jmr.2016.212 Published online by Cambridge University Press

Ag nanopowders to fabricate bulk NC Ag without significant influence of surface oxide layers.[25] Y.Q. Fu et al.[31] have reported that Ag nanopowders can be consolidated at low pressure (34 MPa). The results indicated that the porosity of the bulk compact decreases significantly with an increase in the sintering temperature, and the maximum strain of the sintered specimen reaches to 15%. I. Marek et al.[32] also obtained bulk NC silver-through selective leaching and SPS methods (with sintering pressure of 80 MPa). The Vickers hardness and the maximum compressive strain of the NC Ag were 155 HV and 20%, respectively. To the best of our knowledge, the microstructures and mechanical properties of the bulk NC Ag fabricated by SPS technique at high sintering pressure has not been reported. In the present study, our strategy is to demonstrate the feasibility of fabricating bulk NC Ag using SPS process under proper temperature range (400–550 °C) and high pressure condition (300 MPa). Furthermore, the microstructure and mechanical properties as well as the electrical conductivity of the bulk NC Ag were investigated.

II. EXPERIMENTAL PROCEDURE

A. Raw materials

The chemical compositions of the original spherical Ag nanopowders (Dekedaoking Technology Co., LTD, Beijing, China) are shown in Table I. Figure 1 shows a scanning electron microscopy (SEM) image and the particle size distribution (PSD) of the Ag powders. The PSD of the nanopowders was analyzed using Image-Pro Plus software.[33] The result indicates that the average particle size of the original Ag powders is about 39.0 nm.

TABLE I. Chemical composition of the original Ag powders.

Chemical elements	Cu	Bi	Fe	Pb	Sb	Ag
Content (wt%)	0.025	0.001	0.002	0.015	0.002	Bal.

B. SPS process

The densification of the bulk NC Ag was performed using DR. SINTER type SPS-3.20 equipment (Sojitz Machinery Corporation, Tokyo, Japan) with pulse duration of 3.3 ms and current on-off ratio of 12:2. The powders were sintered in a 0.5 Pa vacuum chamber, using a cylindrical refractory steel die. The external diameter, internal diameter, and height of the die were 55, 25, and 50 mm, respectively. A preload of about 1 MPa was applied on the plunger before sintering, and the heating rate was set as 100 °C/min. The specimens were sintered at different temperatures of 400, 450, 500, and 550 °C, respectively. The holding compressive pressure level was 300 MPa. The sintering temperature was measured using a thermocouple. After soaking the powders at a desired temperature for 5 min, the applied current was reduced, and the specimen was cooled down to room temperature in the furnace. The uniaxial pressure was gradually released during cooling. Disc-shaped samples with 25 mm in diameter and 6 mm in thickness were obtained. Figure 2 shows the shape and size of the NC silver sample prepared by SPS.

C. Characterization tests

The density of the sintered samples was measured by Archimedes' method. The micro-hardness characterization of the NC Ag was carried out by a Vickers hardness tester (VMHT30M, LECO Corporation, San Jose, USA) using a load of 0.98 N (100 gf) and a dwell time of 10 s. Phase analysis of the NC Ag was carried out with x-ray Diffractmeter (X′ Pert PRO MPD, PANalytical B.V., Netherlands) at room temperature. Microstructure of the NC Ag was investigated by field-emission scanning electron microscopy (FESEM, Hitachi S-4800N, Japan) and high-resolution transmission electron microscopy (HRTEM, Philips Tecnai G2 F20, Netherlands). The electrical conductivity was measured using a Sigmatest 2.069 apparatus (Foerster Instruments, Pittsburgh, PA, USA) with a Φ8 mm measuring sensor at a frequency of

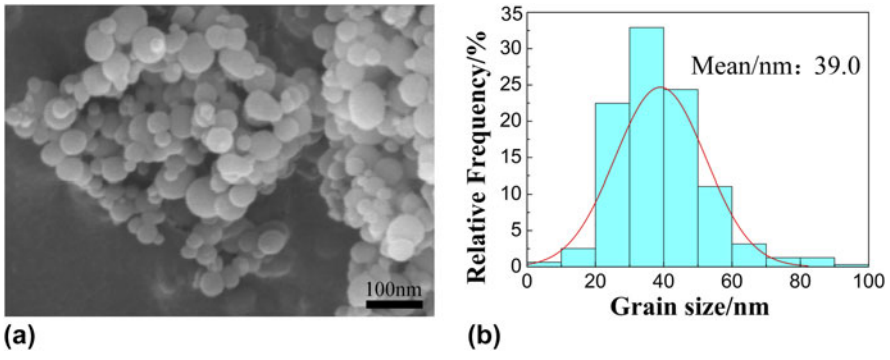


FIG. 1. SEM micrograph of nano Ag powders (a) and the corresponding PSD (b).

https://doi.org/10.1557/jmr.2016.212 Published online by Cambridge University Press

60 kHz. The quasistatic compressive and tensile tests were carried out using a uniaxial servohydraulic testing machine (YHS–229WJ–30T, Shanghai, China) at a constant strain rate of 1.0×10^{-3} s^{-1}. At least five specimens were tested for each mechanical evaluation, and the average values were reported.

III. RESULTS

A. X-ray diffraction (XRD) analysis

Figure 3 shows the XRD patterns of the NC Ag sintered at different sintering temperatures. It can be seen that there is no obvious difference in lattice parameter of the bulk NC Ag sintered at different temperatures. Furthermore, the patterns show that no phase transformation occurred and no impurities were introduced into the nanomaterials during the sintering process. M.A. Meyers et al.[34] have considered that the impurities led to an adverse effect on the mechanical properties of NC materials. Therefore, the NC Ag fabricated by SPS process should have good mechanical properties due to the lack of impurities. The grain size of the NC Ag sintered at different temperatures was calculated using Scherrer's formula based on the XRD data.[35] The corresponding data are about 43.9, 45.2, 45.5, and 114.8 nm, respectively. The results show that there is no striking difference between the sintered samples in the grain size when the sintering temperature is not higher than 500 °C. However, the grains started to grow rapidly as the sintering temperature exceeded 500 °C.

B. Density

Table II displays the density of specimens sintered at different temperatures. It reveals that the density increases with sintering temperature. The growth rate is relatively large as the temperature increases from 400 °C to 500 °C. However, the density of the NC Ag increases slowly when the sintering temperature exceeds 500 °C.

C. Microstructure

Figure 4 exhibits the etched surface of the NC Ag sintered at different temperatures. It can be seen that the intergranular pores in the NC Ag reduce gradually with an increase in sintering temperature. Few pores were detected in the NC Ag sintered at 550 °C. Figure 4 also suggests that the grains of the NC Ag grow slowly when sintering temperature is lower than 500 °C. However, the grain size of the NC Ag sintered at 550 °C is larger than that of the specimens sintered at other temperatures. The PSD histograms of the NC Ag are shown in Fig. 5. The PSD histograms of the NC Ag were analyzed using Image-Pro Plus software. The statistical results reveal that the average grain sizes of the NC Ag sintered at different temperatures are 39.5, 41.2, 41.8, and 122.6 nm respectively. Clearly, the results are consistent with the calculated ones obtained from the XRD data. Therefore, it can be concluded that the sintering temperature should not exceed 500 °C to fabricate the desired NC Ag using SPS technique.

Moreover, Fig. 6 displays a bright-field TEM image of the bulk compact sintered at 500 °C, where many



FIG. 2. Bulk silver compact sintered by SPS process.

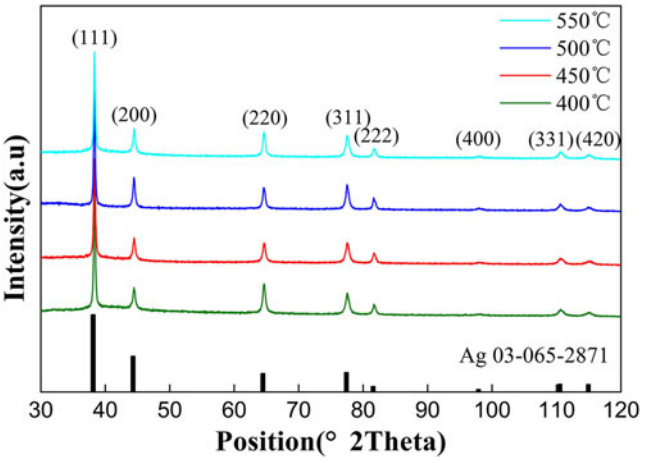


FIG. 3. XRD patterns of the sintered specimens.

TABLE II. Density of the sintered samples.

Sintering temperature (°C)	400	450	500	550
Density (g/cm^3)	9.7	9.9	10.2	10.3
Relative density (%)	92.5	94.4	97.2	98.2

https://doi.org/10.1557/jmr.2016.212 Published online by Cambridge University Press

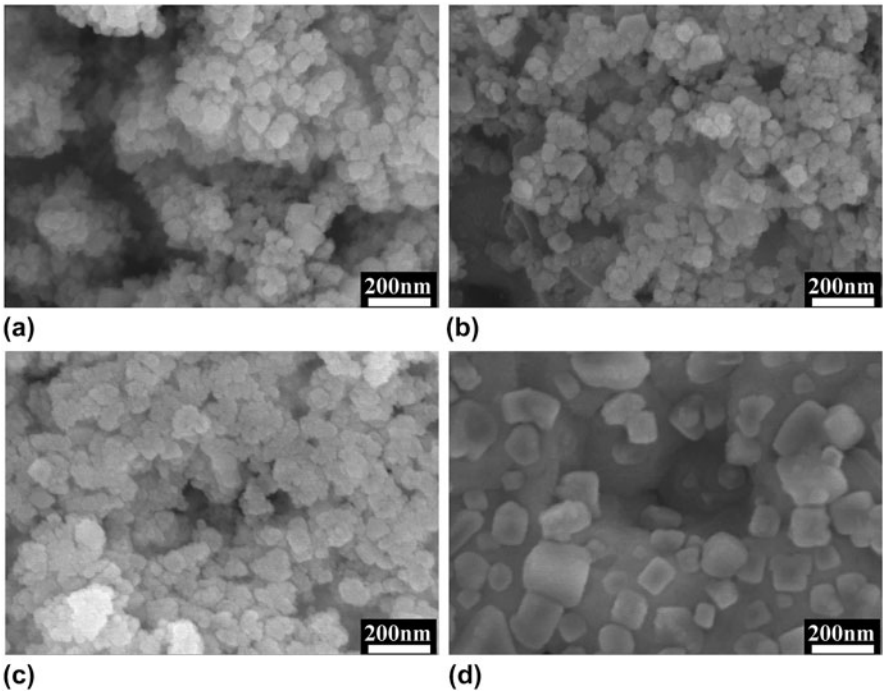


FIG. 4. Microstructure of the NC Ag fabricated by SPS process at different temperature of (a) 400 °C, (b) 450 °C, (c) 500 °C, and (d) 550 °C.

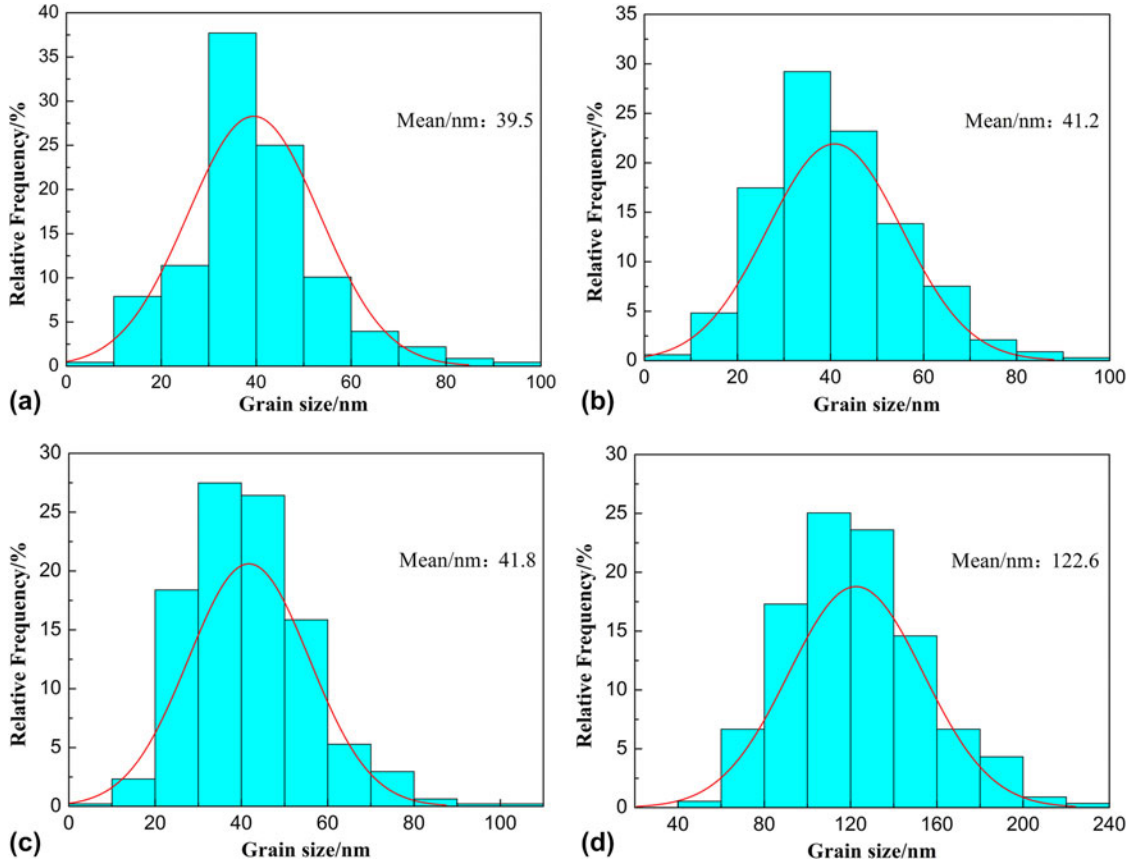


FIG. 5. PSD histogram of the NC Ag fabricated at different temperature of (a) 400 °C, (b) 450 °C, (c) 500 °C, and (d) 550 °C.

https://doi.org/10.1557/jmr.2016.212 Published online by Cambridge University Press

nanoscale grains can be observed. These nanoscale grains contain various lattice defects, such as stacking faults and nanoscale twinning, which is the typical microstructure characteristic of NC bulk materials produced by SPS process.[36] Fig. 7 shows nanoscale twins and corresponding selected area electron diffraction (SAED) pattern. Figure 7(a) indicates that the spacing of nanoscale twins is less than 15 nm. Figure 7(b) depicts the SAED pattern for the corresponding analyzed area, further confirming the presence of nanotwins in the microstructure of NC Ag fabricated using SPS process. Y.T. Zhu et al.[37] and X.Y. Li et al.[38] have proved that the twins are easily formed in FCC metals with low stacking fault energy. As discussed by Y.T. Zhu et al.,[39] the interaction between the twin boundary and dislocations has a positive effect on the mechanical properties of bulk NC materials.

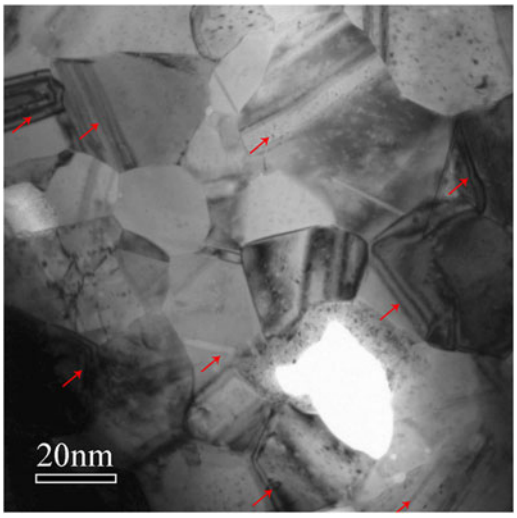


FIG. 6. Bright-field TEM image of NC Ag sintered at 500 °C.

Figure 8 displays the HRTEM image of the NC Ag. The image clearly exhibits a marked twin boundary. The plane spacing of (200) and (111) planes is 2.01 Å and 2.34 Å, respectively. Both of them are smaller than that of the common Ag with coarse grains (2.04 Å and 2.36 Å, respectively). The result indicates that the lattice distortion occur in the NC Ag bulk fabricated by SPS process.[40]

D. Electrical conductivity and micro-hardness

The electrical conductivity and Vickers micro-hardness of the NC Ag sintered at different temperatures is presented in Fig. 9. The electrical conductivity of the NC bulks increases from 72.5% to 82.2% IACS (International Annealed Copper Standard) with increasing sintering temperature from 400 to 550 °C. In addition, the electrical conductivity increases rapidly with the sintering temperature under 450 °C. The electrical conductivity depends on the formation of contacts between contiguous conductive particles. In the SPS process, the relative density of NC silver increase when the sintering temperature climbs from 400 to 450 °C, followed by a rapidly increasing electrical conductivity. When the sintering temperature exceeds 450 °C, the density of the NC Ag continues to increase, but at a slower rate. Thus, the difference of conductivities is minor between the NC Ag sintered at 450, 500, and 550 °C. In addition, the electrical conductivities of all the sintered samples are lower than that of the standard pure Ag (108.4% IACS). The reason may be that electrons movement is blocked in the NC bulk Ag. It is well known that the conductivity depends on the density of charge carrier. The large volume fraction of grain boundaries in the NC Ag can enhance the scattering of electrons, consequently reduces the density of charge carrier. Besides, the small size effect of NC materials also leads to a certain limit effect on the movement of the charge carriers.[41,42]

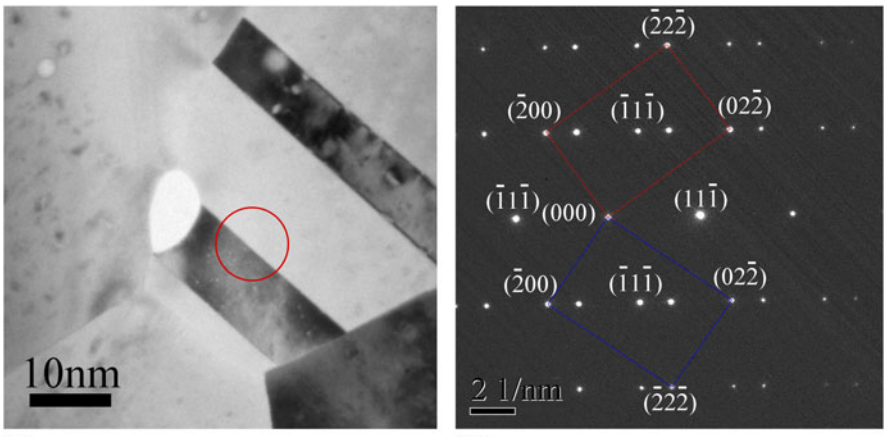


FIG. 7. Bright-field TEM image showing nanoscale twinning, (a) Nanoscale twinning, (b) SAED pattern for the corresponding analyzed area.

https://doi.org/10.1557/jmr.2016.212 Published online by Cambridge University Press

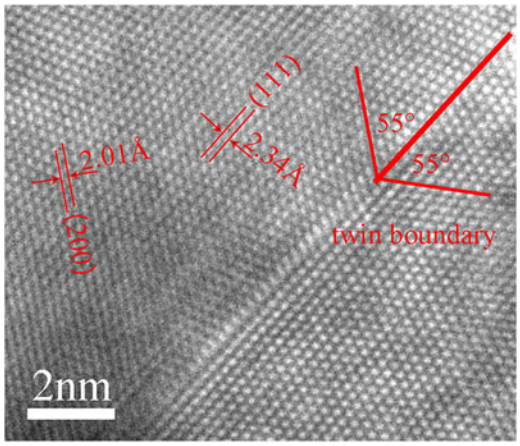


FIG. 8. HRTEM image of NC Ag showing twin boundary and interplanar spacing.

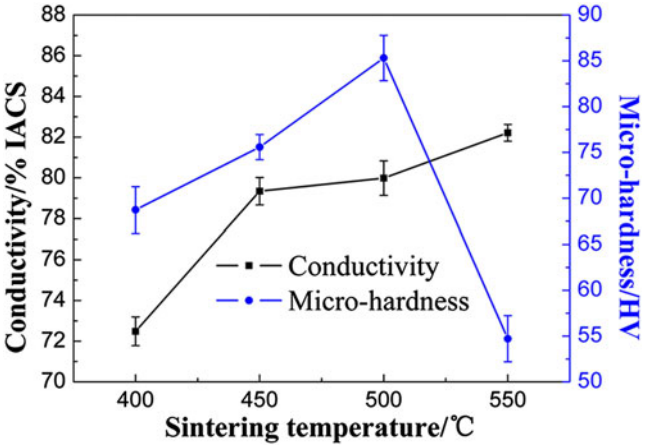


FIG. 9. Curves of electrical conductivity and micro-hardness of NC Ag sintered at different sintering temperature.

Figure 9 also shows that the micro-hardness increases first and then decreases with increasing sintering temperature. The micro-hardness of NC Ag bulk compact sintered at 500 °C reaches 85.3 HV. A sharp decrease in the micro-hardness occurred when the sintering temperature exceeded 500 °C. Both the localized melting and the rapid grain growth of NC Ag should be the primary cause.

E. Mechanical properties

Mechanical properties of NC silver are characterized by compressive and tensile experiments. Figure 10 shows the engineering stress–strain curves of the NC Ag samples sintered at different temperatures. Compression yield strength (CYS) and ultimate tensile strength (UTS) of the NC Ag is enumerated in Table III. The CYS of the NC Ag increases continuously as increasing sintering temperature from 400 to 500 °C, and gets a maximum value of 379 MPa. The CYS of the NC Ag sintered at

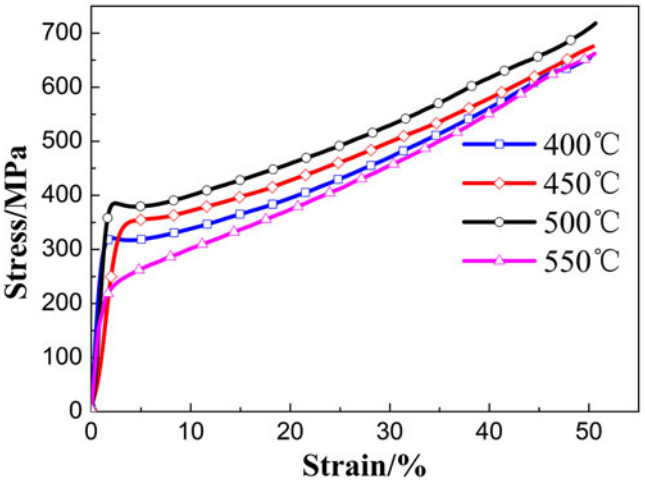


FIG. 10. The engineering stress–strain curves of the NC Ag.

TABLE III. CYS and UTS of the NC Ag.

Sintering temperature (°C)	CYS/MPa	UTS/MPa
400	317 ± 6	412 ± 8
450	352 ± 2	474 ± 3
500	379 ± 5	535 ± 5
550	174 ± 3	258 ± 5

500 °C is about 4 times higher than that of the coarse grained silver (~80 MPa). The high strength of the NC Ag sintered at 500 °C should be attributed to the avoidance of the growth of Ag nanocrystals and the appearance of the nanoscale twinning in the sintering process. However, there is a rapid drop in the CYS when the sintering temperature reaches 550 °C. This phenomenon can easily be explained by the rapid growth of the Ag grains [Fig. 4(d)]. Besides, the UTS shows a similar changing trend as the CYS from Table III. The NC Ag sintered at 500 °C has maximum UTS of 535 MPa due to the appropriate crystallite size and sufficient bonding of the particles. However, the UTS of the NC Ag sample sintered at 550 °C is only 258 MPa due to the quick grain growth.

F. Fracture morphology

Fracture is a complicated dynamic process of initiation, propagation, and coalescence of micropores or microcracks. In the NC Ag produced by SPS, two kinds of fracture morphologies (cleavage fracture and dimple fracture) are observed, as shown in Fig. 11. The surface morphology of the bulk NC Ag sintered at 400 °C shows a mixture of cleavage facets and dimples. These features are attributed to the low sintering temperature and low density. The cleavage fracture disappears as the sintering temperature exceeded 400 °C. The dimple fracture can be observed clearly in NC Ag sintered at 450, 500, and 550 °C, which is the typical fracture morphology feature

https://doi.org/10.1557/jmr.2016.212 Published online by Cambridge University Press

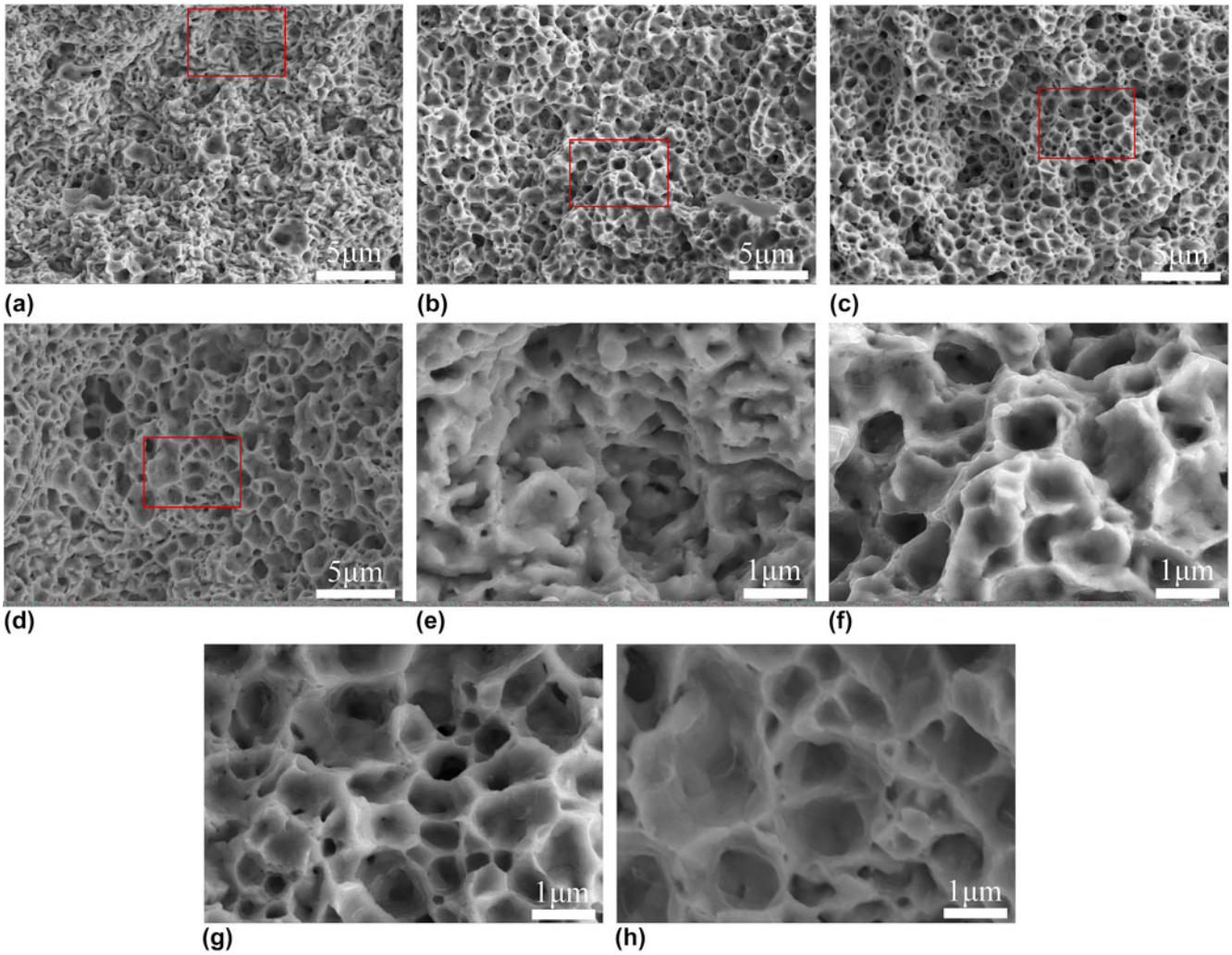


FIG. 11. Fracture morphology of specimens at different sintering temperatures of (a) 400 °C, (b) 450 °C, (c) 500 °C and (d) 550 °C; (e), (f), (g), and (h) are the corresponding higher magnification micrographs.

of ductile materials. In addition, the dimples of NC Ag sintered at different sintering temperatures have different characteristics. The fracture surface of the sample sintered at 500 °C consists of small and shallow dimples, while the fracture surface of the sample sintered at 550 °C contains lots of large and deep dimples. This transition of dimple morphologies is caused by the rapid grain growth.

As shown in Figs. 11(b)–11(d), the pores located at the bottom of the dimples are the starting points for fracture. Since the starting points of fracture have the same distribution, the fracture morphologies of the NC Ag sintered at 450, 500, and 550 °C are similar. However, the dimple sizes of the NC Ag sintered at 450, 500, and 550 °C are 0.85, 0.68, and 1.51 μm, respectively. The dimple sizes of the samples are noticeably greater than the grain sizes. M.A. Meyers et al.[34] and K.S. Kumar et al.[43] have explained this phenomenon through the mechanism of void initiation. The spacing of initiation sites, which is larger than the grain size, determines the dimple size. Nanotwins located in grain boundaries and triple junctions can accelerate nucleation of voids and formation of the void sheets, reducing the spacing of initiation sites. The sizes of dimples decrease as the sintering temperature rises from 450 to 500 °C should be attributed to the twin formation and growing. However, the growth twin is no longer the main factor, the rapid grain growth of the NC Ag sintered at 550 °C leads to an increase in the dimple sizes.

IV. DISCUSSION

In this work, we have investigated the microstructures and properties of NC Ag samples fabricated by SPS process at different sintering temperatures. The results are closely related to the densification mechanism of silver powder during the sintering process. The description of the sintering process can be divided into four stages on the basis of the evolution of the microstructures: activation of the powder, appearance of the sintering neck, growth of

https://doi.org/10.1557/jmr.2016.212 Published online by Cambridge University Press

the neck, and rapid densification.[24] To get more insight into the densification behavior of the NC materials during SPS, the displacement rate of the punch was monitored during sintering process.

Figure 12 presents the variation of temperature, punch displacement rate, and pressure with time during sintering of silver powder at 500 °C. The figure indicates that almost all of the total punch displacement takes place during heating stage of the sintering cycle with negligible punch displacement during holding stage. As shown in Fig. 12, three peaks are observed in the curve of punch displacement rate with time during sintering of silver powder at 500 °C. During the initial sintering stage, the peak I appeared in curve of displacement rate, probably due to the release of gases in powder. Also, the sintering neck will emerge from the surface of the particles because of the spark discharge effect. As the sintering process proceeds, the increase of local temperature among particles was caused by the long spark discharge effect, and the sintering necks will grow up, contact and connect due to the combined effect of evaporation and condensation, the result leads to the emergence of peak II. Then, the sintering pressure is applied while the highest peak III is observed in Fig. 12. The result shows that bulk compact is densified quickly because of the increasing temperature and applied pressure. This suggests that the heating stage of sintering cycle plays an important role in the densification of the compacts while holding stage of sintering cycle is primarily characterized by structural transformations such as the forming of nanotwins.

We concluded that the microstructure and properties of sintered specimens are determined by the sintering temperature and pressure in the holding stage based on the description of the results section. First, the effect of sintering temperature on the density and grain size of Ag samples has been described in Table II and Fig. 4. We analyzed the relationship between the properties of sintered samples and the sintering temperature, and the results are shown in Figs. 5, 9 and 10. Second, we are focused on the influence of sintering pressure on the properties and microstructures of Ag samples. On the one hand, the densification of the samples is enhanced due to applied pressure, which is similar to the effect of sintering temperature. On the other hand, the grain growth is prevented while nanoscale twinning structure is formed as shown in Figs. 6 and 7, which should be attributed to the large applied pressure in the sintering process rather than low pressure reported in the literature.[31,32] The nanoscale twinning exerted great function in enhancing the mechanical properties of the NC silver, especially for improving the ductility.

In general, the strength of NC materials is very high but the ductility is poor due to the restricted dislocation motion in nanostructured grains.[5] Moreover, poor plasticity is a common problem of NC metals or alloys fabricated by SPS as previously reported.[32,44,45] Not only that, a small amount of unavoidable pores and microcracks exist in the bulk NC Ag samples (Fig. 4). However, the NC Ag sintered by SPS process exhibits high ductility during the plastic deformation as shown in Fig. 10. It has been reported that the effect of twinning in NC materials leads to a desirable tendency: the synchronous improvement of strength and plasticity.[46] The special features of nanoscale twinning and its effective cooperation with dislocation slipping work together, changing the balanced relationship between strength and ductility into a synchronous one. So, it has been speculated that the twin boundaries and ultra-fine/submicron grains in the bulk NC Ag could provide a large number of excess dislocations for slipping and even enable the grains to slide or rotate under stress, leading to the synchronous increase in ductility and strength of the bulk NC Ag.

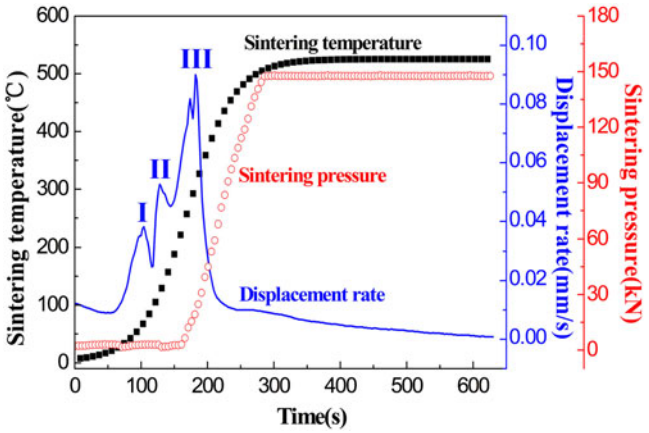


FIG. 12. Typical variation of temperature, displacement rate and pressure with time during sintering of silver powder at 500 °C.

V. CONCLUSIONS

Bulk NC Ag compacts were fabricated by SPS at different sintering temperature and high pressure conditions. The results show that no impurities were introduced in the sintered samples during the sintering process. The density and the electrical conductivity of the NC Ag increase with increasing sintering temperature, while the micro-hardness and UTS of the NC Ag bulks increase initially and then decrease. The NC Ag sintered at 500 °C exhibits the highest micro-hardness of 85.3 HV, the best CYS of 379 MPa and the highest UTS of 535 MPa. Many nanoscale grains can be observed in TEM image of the sintered NC Ag. These nanoscale grains contain various lattice defects, such as stacking faults and nanoscale twinning, which is the typical microstructure characteristic of NC bulk materials produced by SPS process at high pressure. The emergence of nanotwins has a decisive contribution to the strength and elongation of the NC Ag.

https://doi.org/10.1557/jmr.2016.212 Published online by Cambridge University Press

The results also indicated that the sinter temperature for fabricating NC Ag with fine and homogeneous microstructure and good mechanical properties through SPS process should be no more than 500 °C.

ACKNOWLEDGMENTS

The authors acknowledge Prof. Hong-Nian Cai and Dr. Wei-Wei Chen for their fruitful discussions and suggestions during the preparation of this manuscript. The study was supported by the National Natural Science Foundation of China (NSFC, China) under Grant Number of 51374039.

REFERENCES

1. H. Gleiter: Nanocrystalline materials. *Prog. Mater. Sci.* **33**, 223 (1989).
2. K. Lu: Nanocrystalline metals crystallized from amorphous solids: Nanocrystallization, structure, and properties. *Mater. Sci. Eng., R* **16**, 161 (1996).
3. Z.F. Liu, Z.H. Zhang, A.V. Korznikov, J.F. Lu, G. Korznikova, and F.C. Wang: A novel and rapid route for synthesizing nanocrystalline aluminum. *Mater. Sci. Eng., A* **615**, 320 (2014).
4. H.M. Wen, T.D. Topping, D. Isheim, D.N. Seidman, and E.J. Lavernia: Strengthening mechanisms in a high-strength bulk nanostructured Cu–Zn–Al alloy processed via cryomilling and spark plasma sintering. *Acta Mater.* **61**, 2769 (2013).
5. B. Srinivasarao, K. Oh-ishi, T. Ohkubo, and K. Hono: Bimodally grained high-strength Fe fabricated by mechanical alloying and spark plasma sintering. *Acta Mater.* **57**, 3277 (2009).
6. Z.F. Liu, Z.H. Zhang, J.F. Lu, A.V. Korznikov, E. Korznikova, and F.C. Wang: Effect of sintering temperature on microstructures and mechanical properties of spark plasma sintered nanocrystalline aluminum. *Mater. Des.* **64**, 625 (2014).
7. G. Liu, G.J. Zhang, F. Jiang, X.D. Ding, Y.J. Sun, J. Sun, and E. Ma: Nanostructured high-strength molybdenum alloys with unprecedented tensile ductility. *Nat. Mater.* **12**, 344 (2013).
8. X.L. Wu, P. Jiang, L. Chen, F.P. Yuan, and Y.T. Zhu: Extraordinary strain hardening by gradient structure. *Proc. Natl. Acad. Sci. USA* **111**, 7197 (2014).
9. H.N. Kou, J. Lu, and Y. Li: High-strength and high-ductility nanostructured and amorphous metallic materials. *Adv. Mater.* **26**, 5518 (2014).
10. K. Lu: Making strong nanomaterials ductile with gradients. *Science* **345**, 1455 (2014).
11. T. Chookajorn, H.A. Murdoch, and C.A. Schuh: Design of stable nanocrystalline alloys. *Science* **337**, 951 (2012).
12. A.A. Mazilkin, B.B. Straumal, E. Rabkin, B. Baretzky, S. Enders, S.G. Protasova, O.A. Kogtenkova, and R.Z. Valiev: Softening of nanostructured Al–Zn and Al–Mg alloys after severe plastic deformation. *Acta Mater.* **54**, 3933 (2006).
13. F.X. Lin, Y.B. Zhang, N.R. Tao, W. Pantleon, and D. Juul Jensen: Effects of heterogeneity on recrystallization kinetics of nanocrystalline copper prepared by dynamic plastic deformation. *Acta Mater.* **72**, 252 (2014).
14. Y.T. Zhu, J.Y. Huang, J. Gubicza, T. Ungár, Y.M. Wang, E. Ma, and R.Z. Valiev: Nanostructures in Ti processed by severe plastic deformation. *J. Mater. Res.* **18**, 1908 (2003).
15. I.J. Beyerlein, N.A. Mara, J.S. Carpenter, T. Nizolek, W.M. Mook, T.A. Wynn, R.J. McCabe, J.R. Mayeur, K. Kang, S. Zheng, J. Wang, and T.M. Pollock: Interface-driven microstructure development and ultra high strength of bulk nanostructured Cu–Nb multilayers fabricated by severe plastic deformation. *J. Mater. Res.* **28**, 1799 (2013).
16. Q. Wei, Z.L. Pan, X.L. Wu, B.E. Schuster, L.J. Kecskes, and R.Z. Valiev: Microstructure and mechanical properties at different length scales and strain rates of nanocrystalline tantalum produced by high-pressure torsion. *Acta Mater.* **59**, 2423 (2011).
17. J.L.M. Rupp, C. Solenthaler, P. Gasser, U.P. Muecke, and L.J. Gauckler: Crystallization of amorphous ceria solid solutions. *Acta Mater.* **55**, 3505 (2007).
18. A. Yazdani, M.J. Hadianfard, and E. Salahinejad: A system dynamics model to estimate energy, temperature, and particle size in planetary ball milling. *J. Alloys Compd.* **555**, 108 (2013).
19. M. Javanbakht, M.J. Hadianfard, and E. Salahinejad: Microstructure and mechanical properties of a new group of nanocrystalline medical-grade stainless steels prepared by powder metallurgy. *J. Alloys Compd.* **624**, 17 (2015).
20. I. Matsui, H. Mori, T. Kawakatsu, Y. Takigawa, T. Uesugi, and K. Higashi: Enhancement in mechanical properties of bulk nanocrystalline Fe–Ni alloys electrodeposited using propionic acid. *Mater. Sci. Eng., A* **607**, 505 (2014).
21. S. Varam, K.V. Rajulapati, and K. Bhanu Sankara Rao: Strain rate sensitivity studies on bulk nanocrystalline aluminium by nanoindentation. *J. Alloys Compd.* **585**, 795 (2014).
22. S.G. Wang, Y.J. Huang, H.B. Han, M. Sun, K. Long, and Z.D. Zhang: The electrochemical corrosion characterization of bulk nanocrystalline aluminium by x-ray photoelectron spectroscopy and ultra-violet photoelectron spectroscopy. *J. Electroanal. Chem.* **724**, 95 (2014).
23. Z.H. Zhang, Z.F. Liu, J.F. Lu, X.B. Shen, F.C. Wang, and Y.D. Wang: The sintering mechanism in spark plasma sintering—Proof of the occurrence of spark discharge. *Scr. Mater.* **81**, 56 (2014).
24. Z.H. Zhang, F.C. Wang, S.K. Lee, Y. Liu, J.W. Cheng, and Y. Liang: Microstructure characteristic, mechanical properties and sintering mechanism of nanocrystalline copper obtained by SPS process. *Mater. Sci. Eng., A* **523**, 134 (2009).
25. L. Zhang, A.M. Elwazri, T. Zimmerly, and M. Brochu: Fabrication of bulk nanostructured silver material from nanopowders using shockwave consolidation technique. *Mater. Sci. Eng., A* **487**, 219 (2008).
26. G.A. Sweet, M. Brochu, R.L. Hexemer, Jr., I.W. Donaldson, and D.P. Bishop: Consolidation of aluminum-based metal matrix composites via spark plasma sintering. *Mater. Sci. Eng., A* **648**, 123 (2015).
27. Z.A. Munir, U. Anselmi-Tamburini, and M. Ohyanagi: The effect of electric field and pressure on the synthesis and consolidation of materials: A review of the spark plasma sintering method. *J. Mater. Sci.* **41**, 763 (2006).
28. G.A. Sweet, M. Brochu, R.L. Hexemer, Jr., I.W. Donaldson, and D.P. Bishop: Microstructure and mechanical properties of air atomized aluminum powder consolidated via spark plasma sintering. *Mater. Sci. Eng., A* **608**, 273 (2014).
29. U. Anselmi-Tamburini, J.E. Garay, Z.A. Munir, A. Tacca, F. Maglia, and G. Spinolo: Spark plasma sintering and characterization of bulk nanostructured fully stabilized zirconia: Part I. Densification studies. *J. Mater. Res.* **19**, 3255 (2004).
30. O. Guillon, J. Gonzalez-Julian, B. Dargatz, T. Kessel, G. Schierning, J. Räthel, and M. Herrmann: Field-assisted sintering technology/spark plasma sintering: Mechanisms, materials, and technology developments. *Adv. Eng. Mater.* **16**, 830 (2014).
31. Y.Q. Fu, C. Shearwood, B. Xu, L.G. Yu, and K.A. Khor: Characterization of spark plasma sintered Ag nanopowders. *Nanotechnology* **21**, 115707 (2010).
32. I. Marek, D. Vojtěch, A. Michalcová, and T.F. Kubatík: High-strength bulk nano-crystalline silver prepared by selective

https://doi.org/10.1557/jmr.2016.212 Published online by Cambridge University Press

leaching combined with spark plasma sintering. *Mater. Sci. Eng., A* **627**, 326 (2015).
33. H. Wu, S.P. Wen, X.L. Wu, K.Y. Gao, H. Huang, W. Wang, and Z.R. Nie: A study of precipitation strengthening and recrystallization behavior in dilute Al–Er–Hf–Zr alloys. *Mater. Sci. Eng., A* **639**, 307 (2015).
34. M.A. Meyers, A. Mishra, and D.J. Benson: Mechanical properties of nanocrystalline materials. *Prog. Mater. Sci.* **51**, 427 (2006).
35. U. Holzwarth and N. Gibson: The Scherrer equation versus the 'Debye-Scherrer equation'. *Nat. Nanotechnol.* **6**, 534 (2011).
36. F. Fellah, F. Schoenstein, A. Dakhlaoui Omrani, S.M. Chérif, G. Dirras, and N. Jouini: Nanostructured cobalt powders synthesised by polyol process and consolidated by spark plasma sintering: Microstructure and mechanical properties. *Mater. Charact.* **69**, 1 (2012).
37. Y.T. Zhu, J. Narayan, J.P. Hirth, S. Mahajan, X.L. Wu, and X.Z. Liao: Formation of single and multiple deformation twins in nanocrystalline fcc metals. *Acta Mater.* **57**, 3763 (2009).
38. X.Y. Li, Y.J. Wei, L. Lu, K. Lu, and H.J. Gao: Dislocation nucleation governed softening and maximum strength in nano-twinned metals. *Nature* **464**, 877 (2010).
39. Y.T. Zhu, X.Z. Liao, and X.L. Wu: Deformation twinning in nanocrystalline materials. *Prog. Mater. Sci.* **57**, 1 (2012).
40. X.H. Yu, J. Rong, Z.L. Zhan, Z. Liu, and J.X. Liu: Effects of grain size and thermodynamic energy on the lattice parameters of metallic nanomaterials. *Mater. Des.* **83**, 159 (2015).
41. P. Barbosa, N.C. Rosero-Navarro, F. Shi, and F.M.L. Figueiredo: Protonic conductivity of nanocrystalline zeolitic imidazolate framework 8. *Electrochim. Acta* **153**, 19 (2015).
42. U.P. Muecke, S. Graf, U. Rhyner, and L.J. Gauckler: Microstructure and electrical conductivity of nanocrystalline nickel- and nickel oxide/gadolinia-doped ceria thin films. *Acta Mater.* **56**, 677 (2008).
43. K.S. Kumar, H. Van Swygenhoven, and S. Suresh: Mechanical behavior of nanocrystalline metals and alloys. *Acta Mater.* **51**, 5743 (2003).
44. T. Hu, K. Ma, T.D. Topping, B. Saller, A. Yousefiani, J.M. Schoenung, and E.J. Lavernia: Improving the tensile ductility and uniform elongation of high-strength ultrafine-grained Al alloys by lowering the grain boundary misorientation angle. *Scr. Mater.* **78–79**, 25 (2014).
45. A.S. Khan, Y.S. Suh, X. Chen, L. Takacs, and H.Y. Zhang: Nanocrystalline aluminum and iron: Mechanical behavior at quasi-static and high strain rates, and constitutive modeling. *Int. J. Plast.* **22**, 195 (2006).
46. R. Liu, Z.J. Zhang, L.L. Li, X.H. An, and Z.F. Zhang: Microscopic mechanisms contributing to the synchronous improvement of strength and plasticity (SISP) for TWIP copper alloys. *Sci. Rep.* **5**, 9550 (2015).

https://doi.org/10.1557/jmr.2016.212 Published online by Cambridge University Press